RSC Advances

PAPER

View Article Online
View Journal | View Issue

Cite this: *RSC Adv.*, 2016, **6**, 90111

NIR-laser-triggered smart full-polymer nanogels for synergic photothermal-/chemo-therapy of tumors†

Zhouqi Meng, Xiaoliang Chen, Zixiao Liu, Shaohua Chen, Nuo Yu, Peiling Wei, Zhigang Chen* and Meifang Zhu*

Received 13th August 2016
Accepted 12th September 2016

DOI: 10.1039/c6ra20432e

www.rsc.org/advances

Near infrared (NIR, λ = 700–1100 nm) laser-triggered drug delivery systems (DDs) have attracted great interest for the synergic photothermal-/chemo-therapy of tumors, and a prerequisite for their development is to obtain biocompatible and efficient nanoplatforms that possess excellent photothermal and controllable (on/off) drug-release abilities. Herein, we have designed and fabricated full-polymer smart nanogels (PNA–CS–PPy–DOX) as novel NIR-DDs, by using polypyrrole (PPy) as the photothermal agent, PNA–chitosan (PNA–CS) with a lower critical solution temperature (LCST) of 42 °C as the carrier and the doxorubicin (DOX) as the model of the anticancer drugs. The aqueous dispersion of PNA–CS–PPy–DOX shows increased photoabsorption with a wavelength from 600 to 1100 nm. The temperature of its aqueous dispersions (PPy concentration: 1–20 μg mL^{-1}) goes up quickly from room-temperature to 32.4–60.3 °C in 5 min under the irradiation of a 915 nm laser (intensity: 2.0 W cm^{-2}), verifying the excellent photothermal performance. To simulate the *in vivo* drug delivery, a typical aqueous PNA–CS–PPy–DOX (~10 mg mL^{-1}) dispersion is covered by chicken skin as the model of biological tissue. After the irradiation of the 915 nm laser (intensity: 2.0 W cm^{-2}), the temperature of the dispersion goes up to higher than 42 °C (LCST of PNA–CS), resulting in the release of the drug. As a result, the cumulative release of DOX from PNA–CS–PPy–DOX increases from 1.67% (at 0 min) to 48.53% (at 14 min of irradiation), indicating the excellent intelligence and controllability. Subsequently, the PNA–CS–PPy–DOX dispersion is injected into the tumor of the mice. Under the irradiation of the 915 nm laser, the cancer cells can be efficiently destroyed, and the tumor suffers significant ablation, indicating the excellent synergic photothermal-/chemo-therapy effects compared with the single photothermal therapy or chemotherapy effect. Therefore, the present PNA–CS–PPy–DOX nanogels have great superiority as a biocompatible and efficient nanoagent for the synergic photothermal-/chemo-therapy of tumors.

1. Introduction

Drug delivery systems (DDs) have been one of the most promising pathways for achieving chemotherapy for cancer treatment, and represent an ever-evolving field for human health care.[1–3] Through the DDs the active substance or drugs reach the target (*e.g.* tissues or organs), requiring a sufficient time and concentration to produce the therapeutic effect.[4] To realize the drug-delivery process, many kinds of nanocarriers have been intensively investigated over the past few decades, including liposomes,[5] micelles,[6] silica,[7] carbon-based nanomaterials,[8] *etc.* However, the drug-delivery process of these carriers always had the emergence of severe toxic side effects on normal tissues, due to the largely premature leakage of the carrier.[9] To reduce and/or avoid the side effects from these DDs, advanced stimuli-responsive devices for drug delivery have recently received tremendous attention,[10] since stimuli-responsive nanocarriers can respond to changes in their ambient environment and then control the release of drugs systemically. The traditional stimuli sources include the endogenous changes (such as pH,[11] enzyme concentration[12]) and exogenous variations (such as temperature,[13] light,[14] electric[15] and magnetic fields[16]).

Among the above stimuli, the external near infrared (NIR, λ = 700–1100 nm) laser induced internal stimuli-responsive DDs (NIR-DDs) have attracted great interest,[17] and they are usually composed of nanocarriers containing photothermal nanoagents (PNs). When the ideal NIR-DDs are injected into the tissue and swallowed by target cancer cells, NIR laser as the non-invasive exogenous stimuli can afford to determine target tissue location and irradiate DDs with controllable intensity

State Key Laboratory for Modification of Chemical Fibers and Polymer Materials, College of Materials Science and Engineering, Donghua University, Shanghai 201620, China. E-mail: zgchen@dhu.edu.cn; zmf@dhu.edu.cn

† Electronic supplementary information (ESI) available: Materials, cell and animal experimental details; size distribution. See DOI: 10.1039/c6ra20432e

and specific directionality. Subsequently, the PNs in NIR-DDs will absorb and convert the laser energy into heat, resulting in the photothermal therapy. Simultaneously, the generated internal local heat will stimulate the nanocarrier in NIR-DDs to deliver the drugs for the chemotherapy. For achieving such smart NIR-DDs, several kinds of nanocomposites have been studied, including Au@polymer,[18,19] Au@liposome,[20,21] Au@micelle,[22] Au@SiO_2,[23] *etc.* Our group has also prepared some kinds of NIR-DDs, such as Cu_9S_5@SiO_2,[24] CuS@polymer,[25] from which the controllable drug delivery and photothermal performance can be remotely triggered by NIR laser. However, it should be noted that semiconductor/metal-based PNs from these DDs can hardly be degraded in human body. Therefore, it needs to further improve the biocompatibility of NIR-DDs with simultaneous photothermal performances and precise control of drug release abilities for simultaneous photothermal-/chemo-therapy of tumor.

It is well known that there are mainly four kinds of PNs, including organic/polymer compounds (*e.g.* indocyanine green dye[26] and polypyrrole[27]), noble metal nanomaterials (*e.g.* gold nanostructures[28–30] and palladium nanosheets[31]), carbon-based nanomaterials (*e.g.* graphene[32] and carbon nanotubes[33]) and semiconductor nanomaterials (*e.g.* CuS,[34] Cu_9S_5,[35] $W_{18}O_{49}$ (ref. 36 and 37) and Cs_xWO_3 (ref. 38) developed by our group). Among these, organic PNs system have some advantages for future therapeutic application as a result of robust biocompatibility. More importantly, it is more convenient to combine the organic PNs with the thermoresponsive polymer nanocarriers such as poly(*N*-isopropylacrylamide) (PNA) for forming the full-polymer NIR-triggered smart DDs. Moreover, PNA have been widely investigated as the thermosensitive drug delivery system,[39] and their lower-critical-solution-temperature (LCST, only ~32–34 °C in aqueous solutions) can be modulated to near human body temperature by adding the biocompatible and biodegradable polymer chitosan (CS).[40–42]

Inspired by above features, herein we have designed and fabricated full-polymer smart nanogels (PNA–CS–PPy–DOX), using the polypyrrole (PPy) as the photothermal agents, poly(*N*-isopropylacrylamide)–chitosan (PNA–CS) with the LCST of 42 °C as the carriers and the doxorubicin (DOX) as the anticancer drug model. The aqueous dispersion of PNA–CS–PPy–DOX shows strong photoabsorption in NIR region. Under the irradiation of 915 nm laser, the temperature of its aqueous dispersion goes up quickly in 5 min. More importantly, when nanogels were injected into the tumor, under the irradiation of 915 nm laser, cancer cells *in vivo* would be efficiently destroyed by the remotely triggered 915 nm laser, in which the laser energy will conversion to *in vivo* heat, leading to the controlled photothermal-/chemo-therapy.

2. Experimental

2.1 Synthesis of PNA–CS nanogels

PNA–CS nanogels were prepared by using the free radical polymerization.[40] In a typical procedure, *N*-isopropylacrylamide (NIPAAm) monomer (8.8 mmol) was dispersed in an aqueous solution (total volume: 100 mL) containing SDS (0.023 mmol) as the emulsifiers and *N*,*N*′-methylenebis(acrylamide) (MBA, 0.126 mmol) as the crosslinker in a round-bottom flask, and the resulting solution was stirred to form the homogeneous dispersion. Then, 10 mL of 2.5 wt% CS dispersion (containing 2.5% v/v acetic acid solution) was added into the above solution. The flask was purged by dry nitrogen in order to remove any oxygen. After 30 min, potassium persulfate (KPS) initiator (0.25 mmol) was added into the above dispersion to initiate a polymerization for 5 h at 70 °C. The obtained poly(*N*-isopropylacrylamide)–chitosan nanogels (PNA–CS) were purified by dialyzing for 3 days (dialysis bag MWCO = 14 kDa).

2.2 Synthesis of PNA–CS–PPy nanogels

To form the PNA–CS–PPy nanogels, PPy were synthesized by the microemulsion polymerization in the presence of PNA–CS. In brief, $FeCl_3 \cdot 6H_2O$ (1.1 mmol) was dissolved into the PNA–CS dispersion (40 mL) in a round-bottom flask, and then the resulting dispersion was stirred to form the polymer/iron cation complex by combining the Fe^{3+} with polymer chain. Meanwhile, the dispersion was purged by dry nitrogen in order to exclude any oxygen at room temperature for 1 hour. When the above dispersion turned faint yellow, the monomer of pyrrole (5 μL) was added into the above mixture under continuously stirring at 5 °C for 4 h. Then a black dispersion of PNA–CS–PPy was obtained. The as-obtained PNA–CS–PPy nanogels were further purified by dialyzing for 3 days (dialysis bag MWCO = 14 kDa) against ultrapure water to remove the unreacted monomer and other reagents. The final product was stored after lyophilizing at −20 °C for later use.

2.3 Drug loading of PNA–CS–PPy nanogels

PNA–CS–PPy nanogels (0.3 g) was added into phosphate buffer saline (PBS) solution (6.4 mL) containing DOX (0.75 mg mL^{-1}). Then the resulted solution was diluted to 30 mL with fresh PBS solution. The mixture was stirred for 48 h at room temperature. The DOX free of encapsulating was removed by centrifuging at 10 000 rpm for 15 min. Then the supernatant solution was collected and its absorbance was determined by measuring the UV-Vis spectrophotometer at 480 nm. The concentration and weight of unloaded DOX were calculated by the absorbance of the standard curve & different concentrations of DOX. The DOX loading weight in PNA–CS–PPy was obtained by the difference between the original and unloaded weights of DOX. The entrapment efficiency (EE w/w%) and loading content (LC, w/w%) of DOX were evaluated from the equations: EE_{DOX} = (DOX-loading weight/initial weight of DOX) × 100%; LC_{DOX} = (DOX-loading weight/weight of PNA–CS–PPy–DOX) × 100%. For comparison, the loading of DOX in PNA–CS–DOX was also performed. To acquire the same LC_{DOX}, the PNA–CS nanogels (0.3 g) was added to phosphate buffer saline (PBS) solution of DOX (7.6 mL, 0.75 mg mL^{-1}) with the other identical conditions. As a result, the LC_{DOX} of PNA–CS–PPy–DOX and PNA–CS–DOX were all 0.7%, and the EE_{DOX} of PNA–CS–PPy–DOX and PNA–CS–DOX were 43.75% and 36.84%, respectively.

2.4 Characterization and measurement

Physical characterization. Size, morphologies and microstructures of the samples were determined by the transmission electron microscope (TEM, JEM-2100F, JEOL Inc., Japan). Particle size measurement was carried out by laser particle size analyzer (Malvern Inc., UK). Fourier transform-infrared (FT-IR) of different samples were obtained by using the attenuated total reflectance (ATR) methods on a NEXUS-670 (Nicolet Inc., USA). Curves of transmittance and UV-vis absorption spectra were acquired using the absorption peak of 670 nm with Lambda 35 spectrometer (Perkin Elmer Inc., USA). Fluorescence spectra were acquired on FluoroMax 4 spectrofluorometer (HORIBA Scientific Inc., USA).

Photothermal measurements. The aqueous dispersion of PNA–CS–PPy with various concentrations (PPy: 1–20 μg mL^{-1}) in the plastic tubes were exposed to 915 nm laser device (intensity: 2.0 W cm^{-2}, 5 min) with the 915 nm semiconductor laser devices (Xi'an Tours Radium Hirsh Laser Technology Co., Ltd., China). The output power were calibrated by a handy optical power meter (Newport mode 1918-C, CA, USA) before work. For comparison, the pure aqueous solution was also measured with the other identical conditions. The temperature of the PNA–CS–PPy aqueous dispersion was monitored and imaged simultaneously by the infrared thermal imaging camera (FLIR-A300, FLIR Systems Inc., USA).

The simulation and measurement of *in vivo* DOX-release switched by NIR laser. Briefly, PBS dispersion (3 mL) of PNA–CS–PPy–DOX (10 mg mL^{-1}, $LC_{DOX} = 0.7\%$) or PNA–CS–DOX (10 mg mL^{-1}, $LC_{DOX} = 0.7\%$) was replaced in glass vials. These bottled dispersions were maintained in 37 °C bath before treatment. Fresh skin (thickness: about 1 mm) from a dead chicken was washed with water and fixed on a plastic support. Chicken skin as the model of biological tissue was inserted between the 915 nm laser device and glass vials, and then bottled dispersions of PNA–CS–PPy–DOX or PNA–CS–DOX were illuminated by 915 nm laser with the intensity of 2.0 W cm^{-2} for the different time (0, 2, 4, 6, 8, 10, 12, and 14 min). After the treatment, each dispersion was centrifuged at 10 000 rpm for 15 min, and the supernatant solution was collected. The concentration of released DOX in the supernatant solution was characterized by measuring their absorbance at 480 nm with the UV-vis spectroscopy. Three replicates were done for each treatment group. Cell and animal experimental details were supplied in ESI.† All animal investigation conformed to the guide for the Care and Use of Laboratory Animals by the U.S. National Institutes of Health (NIH Publication no. 86-23, revised 1985) and performed in accordance with the protocols approved by the Animal Welfare and Research Ethics Committee of Donghua University.

3. Results and discussion

3.1 Synthesis and characterization of smart nanogel

To obtain NIR-laser-driven DDs (NIR-DDs) with unique intelligence, in the present work we have designed PNA–CS–PPy–DOX nanogels, where the polypyrrole (PPy) was used as the photothermal agents, poly(*N*-isopropylacrylamide)–chitosan (PNA–CS) as the carriers and the doxorubicin (DOX) as the anticancer drug model. The synthesis of PNA–CS–PPy–DOX nanogels consisted of three steps, as demonstrated in Fig. 1.

The first step (step 1 in Fig. 1) was to prepare thermosensitive PNA–CS nanogels by a simply free radical polymerization reaction with KPS as the radical initiator and MBA as a cross-linking agent, according to the previous reports.[40] Fig. 2a presents TEM image of PNA–CS nanogels. Obviously, PNA–CS nanogels are spheral nanoparticles with diameter of ~63 ± 12 nm, which are close to the average hydrodynamic diameter of ~70 nm (Fig. S1†).

To bring the photothermal effects, in the second step (as step 2 in Fig. 1), the biocompatible organic nanoparticles PPy as the PNs were prepared in PNA–CS by microemulsion polymerization method at ice-bath, where the Fe^{3+} was served as the oxidizing agent and the PNA–CS as the stabilizer.[43] From TEM image (Fig. 2b) of PNA–CS–PPy nanogels, we find that almost no single PPy can be found outside of the nanogels, while most of PPy nanoparticles are well existed in the PNA–CS nanogels with diameter of ~20 ± 6 nm. This should be induced from the fact that the metal cations were more easy to bind with the cross-linked PNA–CS chain by an ion–dipole interaction to form the polymer/iron cation complex in the polymerization. When the monomer of pyrrole were introduced into the aqueous dispersion of the cation complex, at the reactive site where the monomer came into contact with the iron cation, it would be more likely to allow the fabrication of PPy nanoparticles in the PNA–CS.[27,44] Moreover, PNA–CS–PPy nanogels exhibit the average hydrodynamic diameter of about ~83 ± 12 nm (Fig. S1†), indicating that the preparation process of PPy has no obvious adverse effect on the diameter of PNA–CS nanogels.

To verify the presence of carriers and PNs in PNA–CS–PPy, FTIR spectra of PNA–CS and PNA–CS–PPy were analyzed (Fig. 2c). For comparison, the spectra of the pure NIPAAm and CS were also investigated. Remarkably, it can be found that the band at 1620 cm^{-1} from NIPAAm is disappeared in PNA–CS, demonstrating the breaking of C=C from NIPAAm monomer after polymerization.[45] The absorption bands among 1560–1660 (such as 1657, 1545) cm^{-1} from NIPAAm and CS are assigned to amide I stretching (C=O) or amide II stretching (N–H) which also remain in PNA–CS structure unit at the same position after polymerization.[40,46] Moreover, PNA–CS sample exhibits a broad and overlapping bands at about 3432 cm^{-1}, due to the O–H symmetric (ν_s) stretching vibrations and amide ν_s(N–H) vibration of CS and NIPAAm.[45,47] The transmission bands at 2971, 2928 and 2872 cm^{-1} are respectively attributed to the

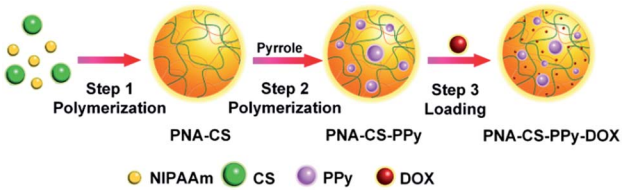

Fig. 1 The synthesis scheme of the PNA–CS–PPy–DOX nanogels.

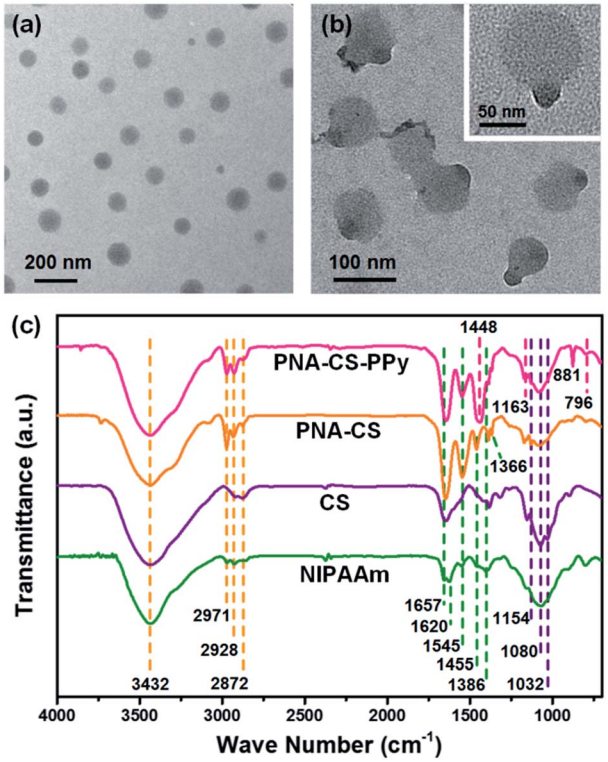

Fig. 2 TEM images of (a) PNA–CS and (b) PNA–CS–PPy nanogels; (c) FTIR spectra of NIPAAm, CS, PNA–CS and PNA–CS–PPy.

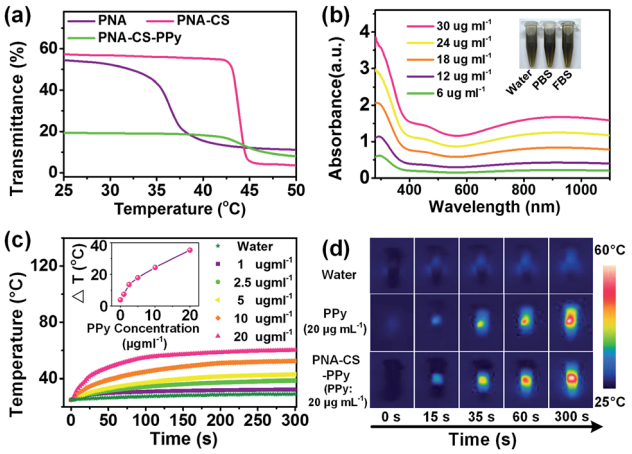

Fig. 3 (a) The transmittance *versus* the temperature of PNA (5 mg mL^{-1}), PNA–CS (5 mg mL^{-1}) and PNA–CS–PPy (3 mg mL^{-1}) aqueous dispersion. (b) UV-vis absorbance spectra of PNA–CS–PPy dispersions with different PPy concentration (6–30 μg mL^{-1}). Inset showing a photograph of PNA–CS–PPy (10 mg mL^{-1}) in different solutions including water, phosphate buffer solution (PBS) and fetal bovine serum (FBS), after stored for several weeks. (c) Temperature elevation of aqueous dispersed PNA–CS–PPy nanogel with different PPy concentration (1–20 μg mL^{-1}) under irradiation with a 915 nm laser at a power density of 2.0 W cm^{-2}. Inset showing the plot of temperature elevation (ΔT) over the 300 s *versus* PPy concentration. (d) Infrared thermal images of water, PPy and PNA–CS–PPy nanogel aqueous dispersion.

asymmetric (ν_s) stretching vibrations of methyl (CH_3), methylene (CH_2) units and $\nu_s(CH_2)$ vibrations.[40] In addition, the peaks at 1455, 1386, and 1366 cm^{-1} are respectively associated with the bending vibration of $-CH_3$ and $-CH_2-$, and methyl groups on $-C(CH_3)_2$ deformation from NIPAAm or CS.[40,45,46] The band at 1154, and 1080/1032 cm^{-1} are assigned to asymmetric (ν_{as}) and symmetric (ν_s) stretching of C–O–C from CS,[40,46] indicating the existence of CS in PNA–CS. After the polymerization of PPy, PNA–CS–PPy spectrum exhibits some new bands besides those of PNA–CS. For example, the bands at 1545 and 1448 cm^{-1} are assigned to typical PPy rings vibrations (Fig. 2c). The absorption bands at 1163 and 1080 cm^{-1} are corresponding to =C–H in plane vibration.[48,49] Additionally, the bands at 881 and 796 cm^{-1} are associated with =C–H out-of-plane vibration. These facts confirm the successful polymerization of pyrrole.[49] Based on the above results, one can conclude that PNA–CS and PNA–CS–PPy have been successful synthesized.

As we know, poly(*N*-isopropylacrylamide) (PNA), with the thermally induced phase behavior, can exhibit a well-defined lower critical solution temperature (LCST) in water. From Fig. 3a, we find that the LCST of the PNA nanogel can reach to ~32 °C, similarity with previous reports.[50] Below LCST, the polymer–water interactions are favorable to allow solubilization. While above LCST hydrophobic polymer–polymer interactions are thermodynamically favored, resulting the rapid swelling and dis-swelling performances, exactly for the controllable drug releasing systems.[51] Herein, for *in vivo* applications of thermosensitive nanogels, it is worthy to be mentioned that the LCST must be tuned to a value above the body temperature (>37 °C) but below the hyperthermia temperature from the photothermal conversion (<43 °C typically).[28] When the CS is added, the LCST of PNA–CS nanogels can be regulated to ~42 °C (Fig. 3a). The shift of LCST is mainly attributed to the fact that the CS plays the role of cross-linker plus serves as a surfactant. This would decreases the mobility of water molecules trapped in cross-linked chain pores, requiring higher amount of heat energy to expel them out.[52–54] Consequently, the LCST shifts in upward direction (>32 °C).[40] Furthermore, after polymerizing the pyrrole in PNA–CS, the LCST of PNA–CS–PPy also remains about 42 °C (Fig. 3a), which is very equal to those of PNA–CS (42 °C), demonstrating that the presence of PPy has negligible effect on the LCST of the thermo-responsive carrier.

PNA–CS–PPy nanogels can be well dispersed in water, phosphate buffer saline (PBS) and fetal bovine serum (FBS) solution. No obvious agglomeration is emerged after be stored for several weeks (the inset of Fig. 3b), demonstrating high stability. The PNA–CS–PPy aqueous dispersions with different PPy concentration (6–30 μg mL^{-1}) exhibit dark color (typical, the inset of Fig. 3b), and their optical properties were studied by using UV-vis-NIR spectroscopy (Fig. 3b). Remarkably, all spectra are similar to that of inorganic NIR PNs in previous reports.[25] PNA–CS–PPy nanogels exhibit a short-wavelength absorption edge at approximately 570 nm. Moreover, the photoabsorption intensity goes up with the increase of wavelength from 600 to ~1000 nm. In particular, the absorption intensity in NIR region (such as, at 900 nm) ascends lineally with PPy concentration in

nanogels (Fig. 3b). These facts confirm that PNA–CS–PPy exhibit the elevated and tuned NIR photoabsorption.

As a result of NIR photoabsorption, PNA–CS–PPy may be used as the photothermal agents. Since PNA–CS–PPy show the strongest absorption around 900 nm, we used 915 nm laser (intensity: 2.0 W cm^{-2}) as the light source to further investigate the photothermal performances (Fig. 3c). The temperature of the PNA–CS–PPy aqueous dispersion (PPy: 1–20 μg mL^{-1}) and its infrared (IR) images were recorded by an infrared thermal camera as a function of irradiated time. For comparison, the temperature of pure water was also determined as the blank test under the other identical conditions. Notably, the blank test illustrates that the temperature of pure water (without PNA–CS–PPy) is only increased by less than 4 °C from the room temperature of 25 °C (Fig. 3c). Correspondingly, the sample of the blank test shows green or blue color, and no remarkably color change can be observed in their IR thermal images as time prolonged (Fig. 3d). When PNA–CS–PPy nanogels are added, the temperature of its aqueous dispersions goes up dramatically under the irradiation of 915 nm laser from 0 to ~100 s, and then exhibits a fairly flat heating-rate from 100 to 200 s, and reaches the maximum at 250–300 s. This temperature elevation process leads to an apparent color change (from blue to red and then became brighter and larger) in IR thermal images, which is similar to that from the pure PPy solution (Fig. 3d). Additionally, from the Fig. 3c, the temperature elevation (ΔT) of PNA–CS–PPy at 300 s is calculated, which ascends almost linearly from 7.4 to 35.3 °C with the increase of PPy concentration from 1–20 μg mL^{-1} (the inset of Fig. 3c). Thus, one can conclude that PPy in the nanogels can rapidly and efficiently convert the NIR laser energy into heat energy, resulting in the rapid temperature elevation.

The last step was to load DOX as the model of anticancer drugs in PNA–CS–PPy nanogels (as step 3 in Fig. 1), since PNA–CS–PPy nanogels have been demonstrated to be excellent drug nanocarriers with zeta potential of −11.6 mV, which has the ability to absorb the DOX (positively charged drugs) by electrostatic interactions. The PNA–CS–PPy nanogels were mixed with DOX for 48 h at room temperature until reaching equilibrium, and then the above mixture was repeatedly washed twice to remove unbounded DOX. The DOX loaded-PNA–CS–PPy (PNA–CS–PPy–DOX) shows the zeta potential of −4.3 mV. For comparison, the DOX loaded-PNA–CS (PNA–CS–DOX) was also investigated under the other identical conditions. As a result, we observe that the original solution of free DOX is red color (the inset of Fig. 4a). After the loading of DOX in PNA–CS–PPy, the color changes from dark brown of PNA–CS–PPy to red-brown of PNA–CS–PPy–DOX. No agglomeration can be observed in PNA–CS–PPy–DOX dispersion after stored for 4 weeks (the inset of Fig. 4a and S2†), verifying good long-term stability. Meanwhile, the loading of DOX also confers the color evolution from colorless of PNA–CS to red of PNA–CS–DOX (the inset of Fig. 4a). Their optical properties were also investigated by UV-vis-NIR spectroscopy (Fig. 4a). The free DOX solution exhibits a typical absorption peak around 480 nm, while PNA–CS–PPy–DOX possesses both the characteristic absorption peak of the DOX in the visible region and broad

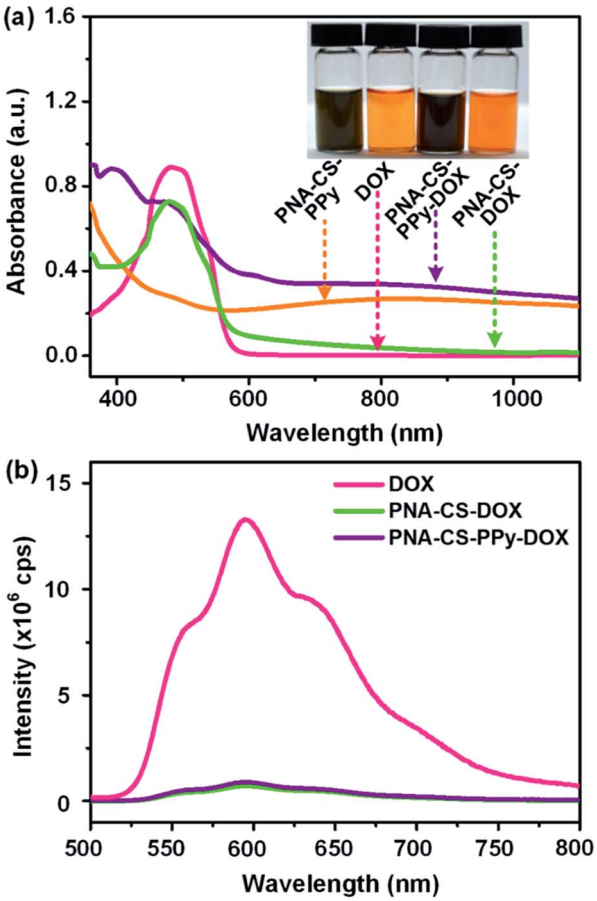

Fig. 4 (a) UV-vis absorbance spectra of the dispersions containing PNA–CS–PPy, free DOX, PNA–CS–PPy–DOX or PNA–CS–DOX; inset showing their photos. (b) Fluorescence spectra of the dispersions of PNA–CS–PPy–DOX (10 mg mL^{-1}), PNA–CS–DOX (10 mg mL^{-1}) and free DOX (100 μg mL^{-1}) with the same concentration of DOX.

plasma absorption band of PNA–CS–PPy in the NIR region (Fig. 4a). Furthermore, both PNA–CS–PPy–DOX and PNA–CS–DOX dispersions show the strong fluorescence quenching if compared with the free DOX solution (Fig. 4b). The above results illustrate that DOX are tightly bounded to PNA–CS–PPy and PNA–CS,[55] inducing the successful loading of DOX. An encapsulation efficiency (EE, w/w%) for DOX within the PNA–CS–PPy and PNA–CS is determined to be 43.75% and 36.84%, respectively.

3.2 The imitation of 915 nm laser triggered controllable drug delivery *in vitro*

For ideal stimuli-responsive DDs, the stimulus should be artificially regulated, and then the drug release can be precisely controlled. The NIR laser as the exogenous stimulus is feasible, since the laser can be remotely tuned (time, intensity, *etc.*) to penetrate the skin/tissue to active the sensitive nanocarriers. To investigate the controllable drug release behavior of PNA–CS–PPy–DOX nanogel *in vivo*, in the present study, we have designed an imitating experiment. Fresh skin (thickness: about 1 mm) from a dead chicken was washed with water, fixed on

a plastic support and then used as the model of biological tissue (Fig. 5a and b). Chicken skin was inserted between the 915 nm laser and PNA–CS–PPy–DOX dispersion in which the loading content of DOX (LC_{DOX}, w/w%) was 0.7%, as shown in Fig. 5c. Subsequently, the 915 nm laser light (intensity: 2.0 W cm^{-2}) was used to penetrate chicken skin to irradiate PNA–CS–PPy–DOX dispersion for different time (0–14 min). It is found that the temperature of the aqueous dispersion can be increased from 25 °C to ~42 °C (at 105 s), even to 47–49 °C (during 200–850 s) in the presence of skin (Fig. 5d). Undoubtedly, the present temperature (47–48 °C) of PNA–CS–PPy–DOX dispersion "*in vivo*" is higher than LCST (~42 °C) of PNA–CS, probably resulting in the volume-shrink of PNA–CS–PPy–DOX and then the release of DOX.

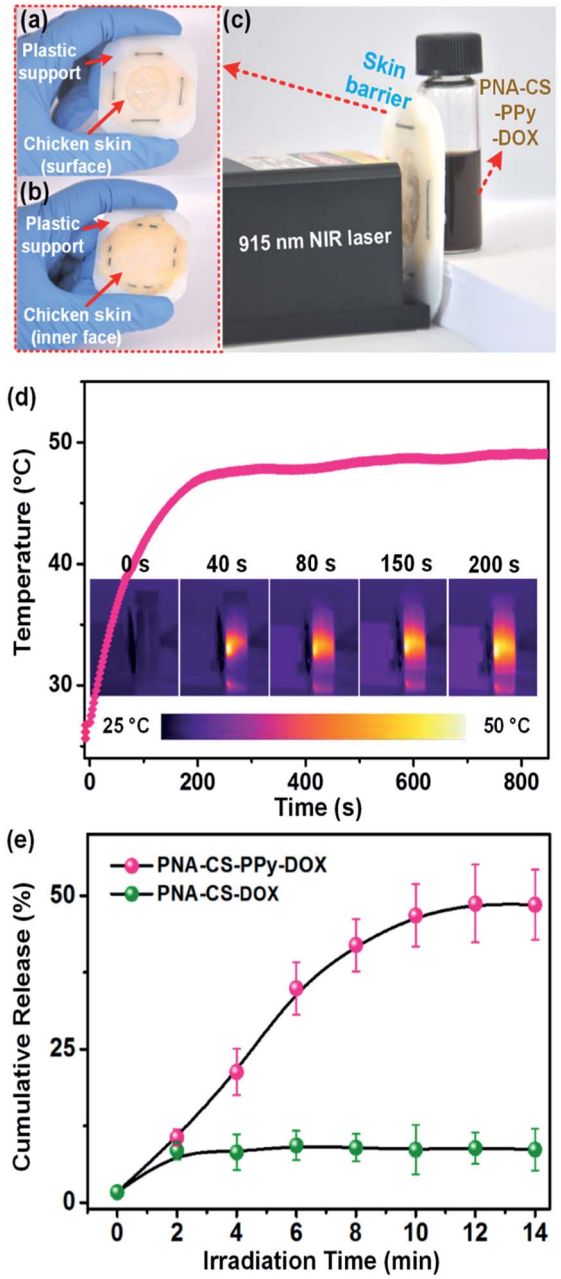

Fig. 5 The imitation of switchable on/off drug release *in vivo*. (a and b) Photos of the chicken skin on a plastic support. (c) Photo of the measuring facility. (d) The temperature elevation of the aqueous dispersion of PNA–CS–PPy–DOX (10 mg mL^{-1}, LC_{DOX} = 0.7%) coated with the chicken skin as a function of irradiation time of 915 nm laser. The insert shows the corresponding infrared thermal images of PNA–CS–PPy nanogel aqueous dispersion. (e) The cumulative release of DOX from the dispersions PNA–CS–PPy–DOX or PNA–CS–DOX under the irradiation of 915 nm laser (2.0 W cm^{-2}) for different time (0–14 min). Error bar are based on at least triplicate measurements.

To determine the release concentration of DOX, the PNA–CS–DOX dispersion was centrifuged after 915 nm laser irradiation, and then their absorbance at 480 nm was measured by the UV-vis spectroscopy. For comparison, the releasing of DOX from PNA–CS–DOX nanogels (without PPy, LC_{DOX} = 0.7%) was also recorded under other identical conditions. Evidently, for PNA–CS–DOX nanogels, the cumulative release of DOX is only 8.44% at 2 min, and remaining almost unchanged in the later time (Fig. 5e). This lower DOX release mainly comes from the spontaneous delivery of PNA–CS–DOX. On the contrary, for PNA–CS–PPy–DOX nanogels, the cumulative release of DOX enhances almost linearly from 1.67% (at 0 min) to 41.94% (at 8 min), and then exhibits a slow increase to 48.53% (at 14 min). Based on the above DOX release results, one can deduce that the drug releasing from the present PNA–CS–PPy–DOX nanogels may be capable of being remotely controlled (turning on/off, rate adjustment, *etc.*) by 915 nm laser (on/off irradiation time, power). More importantly, this NIR laser induced controllable drug delivery behavior can bring not only the effective chemotherapy, but also the photothermal therapy for future synergic cancer treatment.

3.3 The toxicity of nanogels and the synergic therapy *in vitro*

As for biological application, nanomaterials should be required nontoxic. To further evaluate the cytotoxicity of PNA–CS–PPy–DOX nanogels, the cancer cell of human HeLa cells with cell counting kit-8 (CCK-8) assay were used to detect their effects on cell proliferation after cultivating 24 h (Fig. 6). Distinctly, there is no significant difference of the cell proliferation in the absence (control) or presence of 0–1.4 mg mL^{-1} PNA–CS–PPy/PNA–CS–PPy–DOX, and the viabilities nearly reach to 90% (per 1 × 10^4 cells). Even when the concentration of PNA–CS–PPy/PNA–CS–PPy–DOX increase to 1.6 mg mL^{-1}, the cell viabilities is also acceptable (>80%). These results demonstrate that the PNA–CS–

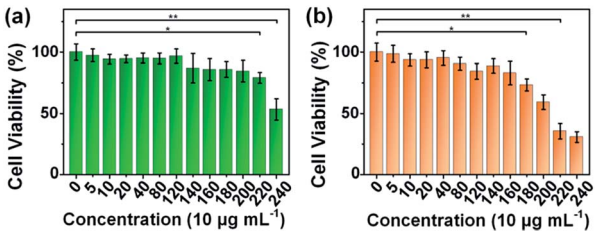

Fig. 6 The viabilities of human HeLa cells incubated with different concentrations of (a) PNA–CS–PPy nanogels and (b) PNA–CS–PPy–DOX nanogels for 24 h, measured by CCK-8 assay. Data represents the mean ± standard deviation of six experiments. *P < 0.05, **P < 0.01.

PPy and PNA–CS–PPy–DOX nanogels aqueous dispersions can be considered to be safety or low cytotoxicity in the concentration of 0–1.6 mg mL^{-1} (per 1×10^4 cells), showing the promising application in biomedicine.

To investigate the synergic photothermal-/chemo-therapy effects *in vitro* from PNA–CS–PPy–DOX, the cells viability was measured after incubated with PNA–CS–PPy–DOX (10 mg mL^{-1}; $LC_{DOX} = 0.7\%$) under the irradiation of 915 nm laser (intensity 2.0 W cm^{-2}) for 6 min (maintaining at 48 °C). For comparison, we also investigated the single chemotherapy effects from free DOX (70 μg mL^{-1}) or delivery DOX (only released from PNA–CS–PPy–DOX), and the single photothermal therapy from PNA–CS–PPy nanogels (10 mg mL^{-1}, Fig. 7). Obviously, the free DOX possesses a high pharmaceutical activity, and only less than 45% cells survive (Fig. 7a). Under the irradiation of 915 nm laser, PNA–CS–PPy group causes a remarkably lower cell viability (<50%), verifying the presence of photothermal therapy effect of PNA–CS–PPy. Similarly, under the laser irradiation, the cell viability from the delivery DOX group also notably goes down (<65%), which should be attributed to the released DOX from PNA–CS–PPy–DOX nanogels, bringing the chemotherapy effect. Very importantly, for PNA–CS–PPy–DOX + NIR group, the cell viability decreases sharply (<25%), which reveals the lowest among all other groups (*vs.* control or delivery DOX, $P < 0.01$; *vs.* PNA–CS–PPy + NIR, $P < 0.05$). Simultaneously, to visually evaluate the viability difference in cellular level, the cells from different groups (PBS, free DOX, delivery DOX, PNA–CS–PPy + NIR, and PNA–CS–PPy–DOX + NIR) were stained with calcein-AM and ethidium homodimer-1 to distinguish live (green) and dead (red) cells (Fig. 7b). Distinctly, in PNA–CS–PPy–DOX + NIR group, the majority of dead cells are observed, which is consistent well with the previous CCK-8 assay of cells proliferation rate. All these results reveal that PNA–CS–PPy–DOX exhibits the excellent synergic photothermal-/chemo-therapy effects which is much better than single photothermal therapy or chemotherapy effect.

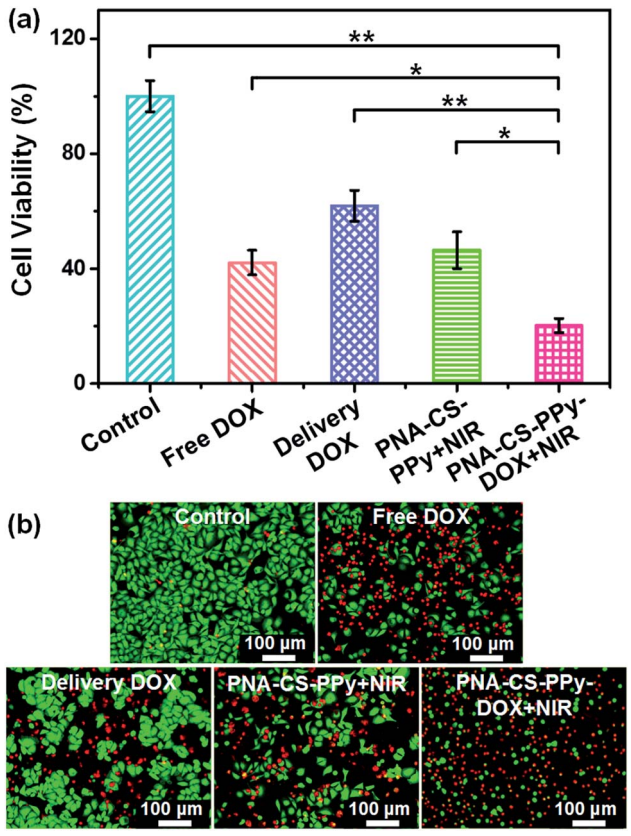

Fig. 7 The synergic therapy effects *in vitro*. (a) Cell viability values (%) from PBS, free DOX (70 μg mL^{-1}), the delivery DOX (released from 10 mg mL^{-1} PNA–CS–PPy–DOX by NIR laser, $LC_{DOX} = 0.7\%$), PNA–CS–PPy (10 mg mL^{-1}) and PNA–CS–PPy–DOX (10 mg mL^{-1}, $LC_{DOX} = 0.7\%$) under the irradiation of 915 nm laser (intensity: 2.0 W cm^{-2}) for 6 min. (b) The confocal images of HeLa cells from different groups. The data are shown as mean ± standard deviation of three experiments, $^*P < 0.05$, $^{**}P < 0.01$.

3.4 The synergic therapy and toxicity *in vivo*

Based on their synergic photothermal-/chemo-therapy *in vitro*, PNA–CS–PPy–DOX nanogels may have great potential as novel nanoagents for the therapy of tumor *in vivo*. HeLa tumor-bearing mice were intratumorally injected with PNA–CS–PPy–DOX (20 mg mL^{-1}, $LC_{DOX} = 0.7\%$) respectively, and then irradiated by 915 nm laser for 10 min (maintaining at 47–48 °C). During 915 nm laser treatment process, the IR thermal camera was employed to monitor the temperature evaluation, and the images were taken at different time intervals (Fig. 8a). For comparison, tumors injected with PBS, DOX, PNA–CS–PPy–DOX (without laser irradiation) and PNA–CS–PPy (irradiated by 915 nm laser) were also investigated under the other identical conditions (Fig. 8). Obviously, for the mice injected with PBS, the surface temperature of the tumor was only elevated by no more than 3.0 °C during the entire treatment (Fig. 8b). And the whole mice body of this group clearly shows green color, and

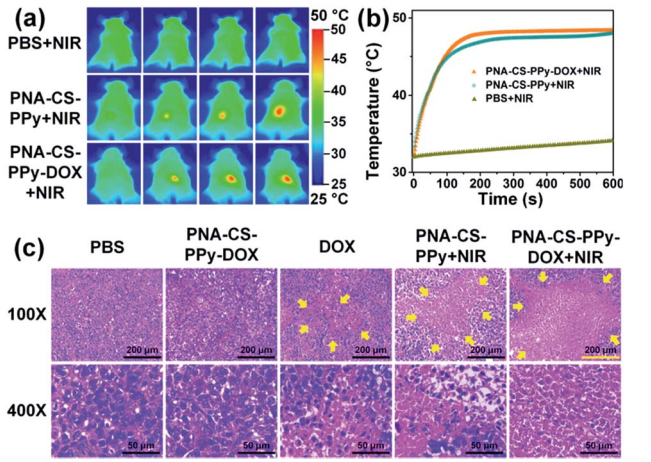

Fig. 8 (a) Infrared thermal image for tumor-bearing mice exposed to the NIR laser (915 nm, 2.0 W cm^{-2}) at post-injection of different agents. (b) The tumor temperatures of mice from (a) monitored by the IR thermal camera during laser irradiation. Color bar on right shows temperature in degrees Celsius. (c) H&E stained tumor sections collected from different group mice at post-treatments. The magnifications are 100× (upper row) and 400× (lower row).

the mice keep a relatively normal physiological temperature distribution (Fig. 8a). While, in the case of PNA–CS–PPy or PNA–CS–PPy–DOX injection, the temperature of tumor surface went up rapidly to reach 47–48 °C (Fig. 8b), and the color of injection region shows the red color and became brighter and larger (Fig. 8a), as demonstrated in Fig. 5. Clearly, the presence of PNA–CS–PPy or PNA–CS–PPy–DOX conferred the efficient temperature elevation of *in vivo* tumor. This fact indicates that 915 nm laser can efficiently penetrate the skin to irradiate PNA–CS–PPy or PNA–CS–PPy–DOX nanogels in tumor, which may bring the therapy effects.

To further evaluate the therapy effect, the mice from different groups were scarified, and tumors were collected and fixed for histological analysis, as shown in H&E stained images (Fig. 8c). For PNA–CS–PPy–DOX group without NIR laser irradiation, cells in their tumors mostly retain their normal morphology with apparent membrane and nuclear structure (compared with PBS group), demonstrating the low cytotoxicity and well biostability of PNA–CS–PPy–DOX nanogels. It should be pointed out that although a small amount of DOX could be spontaneously released from PNA–CS–PPy–DOX nanogels (without NIR laser, Fig. 5c), the very lower dose of DOX can not cause an effective ablation for tumor cells. Furthermore, for DOX or PNA–CS–PPy + NIR groups, there are some segmental damaged areas in 100× magnification (arrows) and a section of pyknotic cells or cytolysis in 400× magnification, indicating that part of cancer cells in mice from PNA–CS–PPy + NIR or DOX group have been destroyed (Fig. 8c). Importantly, for PNA–CS–PPy–DOX + NIR group, one can find the largest damaged areas in 100× magnification (arrows), and a majority of cancer cells are severely necrotized. In particular, from the image at 400× magnification, the maximum cytolysis and the loss of cell morphology are clearly observed. This result arouse from the fact that PNA–CS–PPy–DOX will convert the 915 nm laser energy to heart, which will lead to the rapid increase of tumor temperature (>42 °C), providing the photothermal ablation of cancer cells *in vivo*. Simultaneously, high temperature (>LCST) would trigger the responsive nanogels to release DOX, leading the chemotherapy effects. More importantly, the synergistic effect from PNA–CS–PPy–DOX nanogels can provide the way to lower the dosage of the DOX by using NIR laser irradiation, in this way, the side-effect induced by high dosage of the drug can be effectively reduced. Therefore, PNA–CS–PPy–DOX nanogels exhibit excellent synergic photothermal-/chemo-therapy effects for cancer cells *in vivo* under the irradiation of NIR laser, far exceeding the effect from the individual treatment.

After above treatments, we further investigate the *in vivo* toxicity of PNA–CS–PPy–DOX nanogels. Haematoxylin and eosin (H&E) staining of the main organs from different groups was carried out, including heart, liver, spleen, lung, and kidney, as showing in Fig. 9. Noticeably, there is no obvious histological lesion or any other negative effect in these histological H&E stained samples, demonstrating that the as-obtained PNA–CS–PPy–DOX nanogels have excellent *in vivo* biocompatibility, which can be used as anticancer agent for tumor therapy.

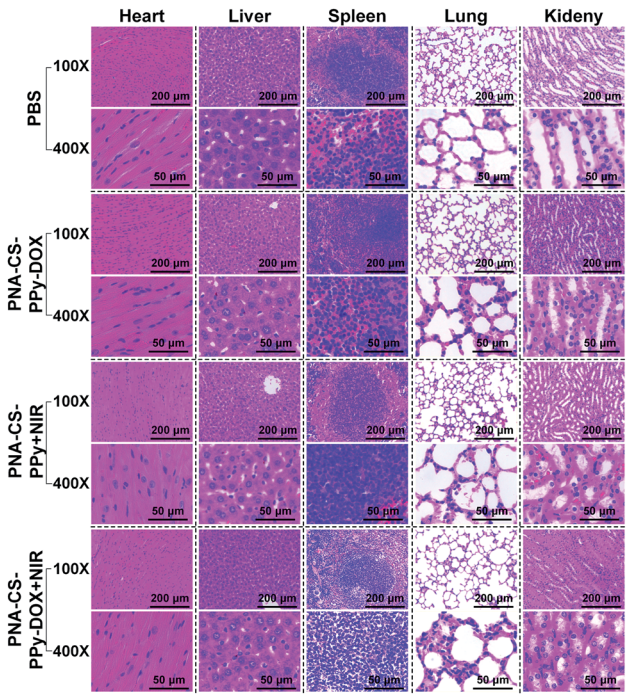

Fig. 9 The H&E stained slices of organs from different groups. Including 100× and 400× magnifications.

4. Conclusion

In summary, the smart full-polymer nanogels of PNA–CS–PPy–DOX have been successfully synthesized. The smart nanogels exhibit strong absorption in NIR region. As a result, the dispersion of nanogels (PPy: 1–20 ppm) shows a rapid temperature elevation of 7.4–35.3 °C in 5 min under the 915 nm laser irradiation. At the same time, the increased temperature (>42 °C) will cause the shrink of temperature-responsive carriers, leading to the precise NIR-triggered drug release. When the PNA–CS–PPy–DOX dispersion is injected into the tumor of the mice, the cancer cell can be efficiently destroyed under the irradiation of 915 nm laser, and the tumor suffer a significant ablation, indicating the excellent synergic photothermal-/chemo-therapy effects compared with the single photothermal therapy or chemotherapy effect. Furthermore, the smart nanogels show the lower cytotoxicity *in vivo*. Therefore, PNA–CS–PPy–DOX nanogels have great superiority as a new kind of biocompatible and efficient anticancer agent for cancer therapeutics. More importantly, this work provides some insights into the design and development of advanced stimuli-responsive nanocomposites for further tumor therapy.

Acknowledgements

This work was financially supported by the National Natural Science Foundation of China (Grant No. 51272299, 51273040, 51473033), Project of the Shanghai Committee of Science and Technology (13JC1400300), the Fundamental Research Funds for the Central Universities, and DHU Distinguished Young Professor Program.

References

1 M. Karimi, A. Ghasemi, P. Sahandi Zangabad, R. Rahighi, S. M. Moosavi Basri, H. Mirshekari, M. Amiri, Z. Shafaei Pishabad, A. Aslani, M. Bozorgomid, D. Ghosh, A. Beyzavi, A. Vaseghi, A. R. Aref, L. Haghani, S. Bahrami and M. R. Hamblin, *Chem. Soc. Rev.*, 2016, **45**, 1457.

2 P. Yang, S. Gai and J. Lin, *Chem. Soc. Rev.*, 2012, **41**, 3679.

3 V. P. Torchilin, *Nat. Rev. Drug Discovery*, 2005, **4**, 145.

4 C. Alvarez Lorenzo and A. Concheiro, *Chem. Commun.*, 2014, **50**, 7743.

5 B. S. Pattni, V. V. Chupin and V. P. Torchilin, *Chem. Rev.*, 2015, **115**, 10938.

6 O. C. Farokhzad and R. Langer, *ACS Nano*, 2009, **3**, 16.

7 F. Hu, Y. Zhang, G. Chen, C. Li and Q. Wang, *Small*, 2015, **11**, 985.

8 C. Cha, S. R. Shin, N. Annabi, M. R. Dokmeci and A. Khademhosseini, *ACS Nano*, 2013, **7**, 2891.

9 J. Croissant and J. I. Zink, *J. Am. Chem. Soc.*, 2012, **134**, 7628.

10 S. Mura, J. Nicolas and P. Couvreur, *Nat. Mater.*, 2013, **12**, 991.

11 Z. Deng, Z. Zhen, X. Hu, S. Wu, Z. Xu and P. K. Chu, *Biomaterials*, 2011, **32**, 4976.

12 L. Zhu, P. Kate and V. P. Torchilin, *ACS Nano*, 2012, **6**, 3491.

13 K. J. Chen, H. F. Liang, H. L. Chen, Y. Wang, P. Y. Cheng, H. L. Liu, Y. Xia and H. W. Sung, *ACS Nano*, 2013, **7**, 438.

14 V. Shanmugam, S. Selvakumar and C.-S. Yeh, *Chem. Soc. Rev.*, 2014, **43**, 6254.

15 H. Kim, S. M. Jeong and J. W. Park, *J. Am. Chem. Soc.*, 2011, **133**, 5206.

16 S. I. Jenkins, M. R. Pickard, N. Granger and D. M. Chari, *ACS Nano*, 2011, **5**, 6527.

17 J. Shi, Y. Jiang, X. Wang, H. Wu, D. Yang, F. Pan, Y. Su and Z. Jiang, *Chem. Soc. Rev.*, 2014, **43**, 5192.

18 W. Wu, J. Shen, P. Banerjee and S. Zhou, *Biomaterials*, 2010, **31**, 7555.

19 Z. Zhang, J. Wang, X. Nie, T. Wen, Y. Ji, X. Wu, Y. Zhao and C. Chen, *J. Am. Chem. Soc.*, 2014, **136**, 7317.

20 A. Agarwal, M. A. Mackey, M. A. El-Sayed and R. V. Bellamkonda, *ACS Nano*, 2011, **5**, 4919.

21 L. J. E. Anderson, E. Hansen, E. Y. Lukianova Hleb, J. H. Hafner and D. O. Lapotko, *J. Controlled Release*, 2010, **144**, 151.

22 Z. Xiao, C. Ji, J. Shi, E. M. Pridgen, J. Frieder, J. Wu and O. C. Farokhzad, *Angew. Chem.*, 2012, **124**, 12023.

23 Y. T. Chang, P. Y. Liao, H. S. Sheu, Y. J. Tseng, F. Y. Cheng and C. S. Yeh, *Adv. Mater.*, 2012, **24**, 3309.

24 G. Song, Q. Wang, Y. Wang, G. Lv, C. Li, R. Zou, Z. Chen, Z. Qin, K. Huo, R. Hu and J. Hu, *Adv. Funct. Mater.*, 2013, **23**, 4281.

25 Z. Meng, F. Wei, R. Wang, M. Xia, Z. Chen, H. Wang and M. Zhu, *Adv. Mater.*, 2016, **28**, 245.

26 J. Yu, D. Javier, M. A. Yaseen, N. Nitin, R. Richards-Kortum, B. Anvari and M. S. Wong, *J. Am. Chem. Soc.*, 2010, **132**, 1929.

27 Z. Zha, X. Yue, Q. Ren and Z. Dai, *Adv. Mater.*, 2013, **25**, 777.

28 M. S. Yavuz, Y. Cheng, J. Chen, C. M. Cobley, Q. Zhang, M. Rycenga, J. Xie, C. Kim, K. H. Song, A. G. Schwartz, L. V. Wang and Y. Xia, *Nat. Mater.*, 2009, **8**, 935.

29 P. Huang, P. Rong, A. Jin, X. Yan, M. G. Zhang, J. Lin, H. Hu, Z. Wang, X. Yue, W. Li, G. Niu, W. Zeng, W. Wang, K. Zhou and X. Chen, *Adv. Mater.*, 2014, **26**, 6401.

30 H. Deng, F. Dai, G. Ma and X. Zhang, *Adv. Mater.*, 2015, **27**, 3645.

31 X. Huang, S. Tang, X. Mu, Y. Dai, G. Chen, Z. Zhou, F. Ruan, Z. Yang and N. Zheng, *Nat. Nanotechnol.*, 2011, **6**, 28.

32 L. Feng, L. Wu and X. Qu, *Adv. Mater.*, 2013, **25**, 168.

33 G. Hong, S. Diao, A. L. Antaris and H. Dai, *Chem. Rev.*, 2015, **115**, 10816.

34 Q. Tian, F. Jiang, R. Zou, Q. Liu, Z. Chen, M. Zhu, S. Yang, J. Wang, J. Wang and J. Hu, *ACS Nano*, 2011, **5**, 9761.

35 Q. Tian, M. Tang, Y. Sun, R. Zou, Z. Chen, M. Zhu, S. Yang, J. Wang, J. Wang and J. Hu, *Adv. Mater.*, 2011, **23**, 3542.

36 Z. Chen, Q. Wang, H. Wang, L. Zhang, G. Song, L. Song, J. Hu, H. Wang, J. Liu, M. Zhu and D. Zhao, *Adv. Mater.*, 2013, **25**, 2095.

37 W. Xu, Q. Tian, Z. Chen, M. Xia, D. K. Macharia, B. Sun, L. Tian, Y. Wang and M. Zhu, *J. Mater. Chem. A*, 2014, **2**, 5594.

38 W. Xu, Z. Meng, N. Yu, Z. Chen, B. Sun, X. Jiang and M. Zhu, *RSC Adv.*, 2015, **5**, 7074.

39 D. Schmaljohann, *Adv. Drug Delivery Rev.*, 2006, **58**, 1655.

40 M. K. Jaiswal, R. Banerjee, P. Pradhan and D. Bahadur, *Colloids Surf., B*, 2010, **81**, 185.

41 Q. Yuan, R. Venkatasubramanian, S. Hein and R. D. K. Misra, *Acta Biomater.*, 2008, **4**, 1024.

42 M. Prabaharan and J. Mano, *Drug Delivery*, 2004, **12**, 41.

43 K. Yang, H. Xu, L. Cheng, C. Sun, J. Wang and Z. Liu, *Adv. Mater.*, 2012, **24**, 5586.

44 J. Y. Hong, H. Yoon and J. Jang, *Small*, 2010, **6**, 679.

45 Y. V. Pan, R. A. Wesley, R. Luginbuhl, D. D. Denton and B. D. Ratner, *Biomacromolecules*, 2001, **2**, 32.

46 A. Pawlak and M. Mucha, *Thermochim. Acta*, 2003, **396**, 153.

47 E. J. Baran, *Carbohydr. Polym.*, 2008, **74**, 704.

48 T. K. Vishnuvardhan, V. R. Kulkarni, C. Basavaraja and S. C. Raghavendra, *Bull. Mater. Sci.*, 2006, **29**, 77.

49 W. Chen, X. Li, G. Xue, Z. Wang and W. Zou, *Appl. Surf. Sci.*, 2003, **218**, 216.

50 C. S. Brazel and N. A. Peppas, *Macromolecules*, 1995, **28**, 8016.

51 S. Sun and P. Wu, *Macromolecules*, 2013, **46**, 236.

52 B. Sierra-Martín, Y. Choi, M. S. Romero-Cano, T. Cosgrove, B. Vincent and A. Fernández-Barbero, *Macromolecules*, 2005, **38**, 10782.

53 Z. Zhao, S. An, H. Xie and Y. Jiang, *Chin. J. Polym. Sci.*, 2015, **33**, 173.

54 Y. Okada and F. Tanaka, *Macromolecules*, 2005, **38**, 4465.

55 C. Wang, H. Xu, C. Liang, Y. Liu, Z. Li, G. Yang, L. Cheng, Y. Li and Z. Liu, *ACS Nano*, 2013, **7**, 6782.